THE JOURNAL OF PHYSICAL CHEMISTRY B

pubs.acs.org/JPCB Article

Computational Modeling of the Disulfide Cross-Linking Reaction

Muhammad A. Hagras, Michael A. Bellucci, Gianpaolo Gobbo, Ryan A. Marek, and Bernhardt L. Trout*

Cite This: https://dx.doi.org/10.1021/acs.jpcb.0c07510 Read Online

ACCESS | Metrics & More | Article Recommendations | Supporting Information

ABSTRACT: Disulfide cross-linking is one of the fundamental covalent bonds that exist prevalently in many biological molecules that is involved in versatile functional activities such as antibody stability, viral assembly, and protein folding. Additionally, it is a crucial factor in various industrial applications. Therefore, a fundamental understanding of its reaction mechanism would help gain insight into its different functional activities. Computational simulation of the disulfide cross-linking reaction with hydrogen peroxide (H_2O_2) was performed at the integrated quantum mechanical/molecular mechanical (QM/MM) level of theory in a water box under periodic boundary conditions. A benchmarking study for the barrier height of the disulfide formation step was performed on a model system between methanethiol and methane sulfenic acid to determine, for the QM system, the best-fit density functional theory (DFT) functional/basis set combination that produces comparable results to a higher-level theory of the coupled-cluster method. Computational results show that the disulfide cross-linking reaction with H_2O_2 reagent can proceed through a one-step or a two-step pathway for the high pK_a cysteines or two different pathways for the low pK_a cysteines to ultimately produce the sulfenic acid/sulfenate intermediate complex. Subsequently, those intermediates react with another neutral/anionic cysteine residue to form the cysteine product. In addition, the solvent-assisted proton-exchange/proton-transfer effects were examined on the energetic barriers for the different transition states, and the molecular contributions of the chemically involved water molecules were studied in detail.

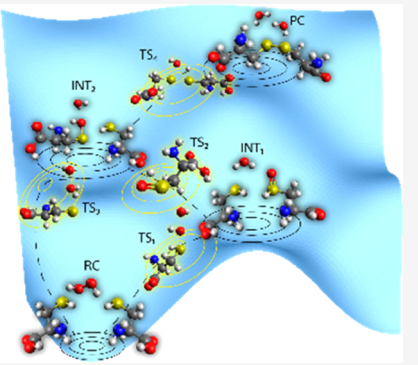

1. INTRODUCTION

Disulfide bridges between pairs of cysteine residues are essential covalent linkages that determine the overall three-dimensional structure of many proteins and their stabilities. For example, disulfide bonds play an essential role in the stability of the human monoclonal antibodies, where they link the two heavy chains and the heavy and light chains.[1−4] Hence, understanding the disulfide bond formation mechanism would represent an important factor in developing new therapeutic monoclonal antibodies, which gain more interest recently due to their inherent target specificity.[5] Additionally, disulfide bonds are also critical in forming various viral proteins and the assembly of viral capsids. Mutation of specific conserved cysteines in virus-like particles (VLP) of human papillomavirus completely prevents VLP assembly.[6] Furthermore, proper disulfide cross-linking is a crucial factor for in vivo protein folding and in vitro refolding[7−12] either by providing structural stability for the folded protein[13] or is pivotal in the folding process itself.[8,9,14−17] Incidentally, under oxidative stress conditions with an abundance of reactive oxygen species (ROS), protein damage occurs through different mechanisms, including oxidation of free thiol groups and reducing native disulfide bridges.[18] Hydrogen peroxide (H_2O_2), one of the ROS species, is rather a weak oxidant but generated as byproducts in various normal aerobic cell metabolism processes such as oxidative phosphorylation reaction and also in other pathological inflammatory conditions.[19]

Additionally, disulfide bonds are one of the crucial factors in various industrial applications. Disulfide bridges are heavily found in antifreeze proteins, vital in cryosurgery and cryopreservation of living tissues.[20−22] The food industry is another example where disulfide bonds play a vital role in the breadmaking process[23] and the gelling of milk proteins and many other proteins.[24,25] Disulfide engineering is another important field where designing novel disulfide bonds increases the half-life stability of the pharmaceutical peptides and the operational functions of industrial enzymes.[26] Like in nature, trace levels of hydrogen peroxide are also present in those complex industrial mixtures, where it is produced as a byproduct through various chemical reactions between the active ingredients, excipients, and impurities.[27−30]

Therefore, the computational study of the disulfide cross-linking reaction between a pair of cysteine residues and H_2O_2 molecule is essential to understand the fundamental characteristics of such an important reaction. This reaction was studied before by many authors.[31−35] In the current study, we extend beyond those reports and systematically explore the different

Received: August 17, 2020
Revised: October 17, 2020

transition states (TS) and local minima structures of the disulfide cross-linking potential energy surface (PES) for low and high pK_a cysteines with a different number of solvent-assisted proton exchanges/proton transfers (SAPE/SAPT). Furthermore, some reports are limited concerning the level of theory, the model used in the study, or the reaction feature under study. In the current study, the full chemically relevant landscape of the disulfide cross-linking PES is systematically explored using a hybrid quantum mechanical/molecular modeling (QM/MM) approach on a model of two cysteine residues and H_2O_2 in an explicit periodic water box. The SAPE/SAPT effects were also examined on the energetic barriers for the different calculated transition states. Such a comprehensive study provides an essential platform for a more complicated simulation, such as studying the environmental effect of the nearby peptide residues on the different energetic barriers of the disulfide cross-linking reaction.

2. COMPUTATIONAL METHODS

2.1. Benchmarking Calculations. A model system of methanethiol (CH_3SH) and methane sulfenic acid (CH_3SOH) was built in vacuum to study the condensation reaction step that produces dimethyl disulfide and a water molecule (Figure S1). The sulfhydryl hydrogen atom and sulfenic acid OH group were manipulated manually to reproduce the transition state (TS) of the disulfide bond formation step. A transition-state search was performed at the high level of theory of coupled-cluster (CCSD)/6-311G** with frozen core orbitals in the NWCHEM 6.6 package.[36] Subsequent frequency calculations were performed to verify the nature of the optimized transition states, which was further confirmed by inspecting the corresponding imaginary frequency eigenvectors (Figure S1). Besides, the same transition state was reproduced using different density functional theory (DFT) functionals/basis set combinations to benchmark against the more accurate results of the CCSD/6-311G** method.

To examine the effect of Hartree−Fock (HF) exact exchange energy, benchmarking simulations were performed with different hybrid DFT functionals (ACM, which has 20% HF exact exchange energy, BECKE98 with 22%, PW6B95 with 28%, M06 with 27%, MPW1B95 with 31%, PBE0 with 25%, and M11 with 42.8%) and a newly built hybrid DFT functional PBE50 (=1/2 E_X^{pbe96} + 1/2 E_X^{HF} + $E_C^{pw91lda}$), which has 50% HF exact energy instead of 25% contribution in the PBE0[37] DFT functional. Subsequent imaginary frequency eigenmode-following geometry optimization was performed on the obtained transition state (and using its frequency Hessian matrix) in both reactant and product directions to compute their energies and determine their structures.

2.2. Transition-State QM/MM Calculations. To calculate the transition states for the neutral cysteine case, we built a model system (M1, Figure S2) of a neutral cysteine residue (where its dangling N- and C-termini are capped by hydrogen atoms), a H_2O_2 molecule, and sixteen QM waters (surrounding the thiol group and H_2O_2 molecule) that are inserted into a 30 Å periodic cubic box of 4350 solvent water molecules. Sixteen water molecules were picked as part of the QM region since up to three waters would be involved in SAPE while the remaining 13 waters are involved in an active hydrogen network with those water molecules, H_2O_2, or the thiol/thiolate groups. Those 13 QM waters represent the first solvation shell, which provides an accurate electronic rearrangement for the chemically active QM atoms involved in each transition state. The QM waters were manipulated manually to ensure a maximum of four hydrogen bonds among those QM waters and the nearby cysteine residue or the hydrogen peroxide molecule. The whole system was classically optimized using the Amber03 force field[38] in the GROMACS 5.1.1 package[39] and then equilibrated at 298.15 K and 1 bar for 30 ns. Afterward, the system was divided into a QM region (which includes the neutral cysteine, the H_2O_2 molecule, and the 16 QM waters) and a MM region (which includes the rest of MM waters), which was optimized at the QM/MM level using PBE50/6-311++G** and the Amber force field in the NWCHEM 6.6 package.[36] Finally, the MM region was classically equilibrated for another 50 ns at 298.15 K and 1 bar with fixed coordinates for the QM region. Hence, the QM region only interacts electrostatically (where it is represented as ESP point charges) and through Van der Waals forces with the MM region. To simulate the reaction pathways forming the disulfide bond, we built a second model system (M2, Figure S3) consisting of a neutral cysteine residue and a sulfenic acid intermediate surrounded by 14 QM water molecules. Up to 2 QM waters are involved in SAPE and the remaining 12 QM waters represent the first solvation shell. The M2 model was inserted in a 30 × 30 × 40 $Å^3$ periodic box of 5188 water solvent molecules and subsequently minimized and equilibrated as above. For calculations of the transition states of anionic cysteines, the previous procedure was repeated on model systems containing anionic cysteines (formal charge = −1.0) instead of neutral cysteines.

To generate the different transition states, we positioned the relevant atoms manually to produce the desired transition state, which then was optimized at the QM/MM level using the PBE50/6-311++G** method and the Amber force field in the NWCHEM 6.6 package, which uses a multiregion iterative optimization procedure:[40] (1) the QM region is optimized with fixed coordinates of the MM atoms where both regions interact electrostatically and through Van der Waals interactions, (2) the electrostatic potential (ESP) fitted charges of the QM atoms are calculated, (3) the MM region is optimized with fixed coordinates of the QM region, which is represented as ESP charges; and (4) the previous steps are repeated until reaching the desired first-order saddle point. We employed an iterative QM/MM transition-state optimization scheme to obtain the lowest TS energy. In that scheme, each QM/MM optimization step proceeds along the same imaginary frequency eigenvector and utilizes the Hessian matrix from the previous QM/MM optimization step. That iterative QM/MM procedure stops when it converges to the lowest TS energy where the change of the TS energy between two consecutive steps is less than 0.1 kcal/mol. A subsequent frequency calculation was performed to verify the nature of the optimized transition state (which was further confirmed by inspecting the corresponding frequency eigenvectors) and to calculate the zero-point vibrational energy, thermal correction to the enthalpy, and total entropy of the Gibbs free energy using the harmonic oscillator approximation method. To generate the corresponding reactant and product complexes (PC) for each calculated transition state, we performed an eigenmode-following geometry optimization on the transition state structure (and using its frequency Hessian matrix) in both reactant and product directions. Atomic partial charges for the various transition, reactant, and product complexes were calculated using the ESP module of NWCHEM with the default settings.

https://dx.doi.org/10.1021/acs.jpcb.0c07510
J. Phys. Chem. B XXXX, XXX, XXX−XXX

Table 1. Benchmarking Results of the Barrier Height for the Disulfide Bond Formation Reaction

	barrier height (kcal/mol)			
DFT functional/basis set	6-311G	6-311G**	6-311++G**	6-311++G(2d,2p)
ACM	28.1	41.6	41.0	
PW6B95	24.2	41.4	41.2	
M06	28.3	43.1	N/A[a]	
MPW1B95	30.3	43.3	42.9	
PBE0	29.0	N/A[a]	42.2	
M11	37.3	50.0	49.7	49.4
PBE50	35.9	51.1	50.6	50.0
BECKE98	28.1	41.1	41.1	41.7

[a]No SCF convergence was obtained.

3. RESULTS AND DISCUSSION

3.1. Benchmarking Results of the Disulfide Bond Formation Reaction.

[CH3SH + CH3SOH → CH3S − SCH3 + H2O]

The main purpose of the benchmarking study is to find a DFT functional/basis set combination that has comparable energy barrier results of the disulfide bond formation step to the more accurate results of a higher level of theory. Coupled-Cluster (with single and double excitations)/6-311G** produced an energy barrier of 55.3 kcal/mol for the disulfide bond formation reaction. Different hybrid DFT functionals and different basis sets were used to calculate the same energy barrier (Table S1 in the Supporting Information and Table 1).

Compared to CCSD, we discovered two significant trends in the DFT results. First, including one set of polarization basis functions dramatically improves the results, as expected for bond formation/breakage reaction. On the other hand, adding a set of diffuse basis functions has a negligible effect on the results. The addition of a second set of polarization basis functions for a subset of DFT functionals (M11, PBE50, and BECKE98) also shows a negligible effect. Second, the higher the contribution of HF exact exchange energy to the DFT exchange energy, the closer the DFT results are to the CCSD one. The Minnesota DFT functional (M11, which includes 42.8% HF energy)[41] shows the best benchmarking result, but due to its inherent slow convergence,[42] we adjusted the PBE0 DFT functional to include 50% HF exact exchange energy (which is then called PBE50), which then shows a comparable energy barrier results to the CCSD method. Ultimately, we decided to use PBE50 with the 6-311++G** basis set to produce the best accuracy at a reasonable computational cost.

3.2. QM/MM Results. Since cysteine residues often exist in the broader environment of proteins, environmental factors (such as positively charged residues, solvation effect, hydrogen bonding, or α-helical dipole moment interaction)[43−45] can potentially lead to pK_a shifts of such cysteine residues to span a pK_a range of 8.2[46−48]−3.5.[49] Hence, in the current study, we investigated the disulfide cross-linking reaction with hydrogen peroxide between two neutral cysteine residues for cysteines with high pK_a values and two anionic cysteine species for low pK_a cysteines.

The cysteine sulfenic acid or its deprotonated sulfenate anion represents necessary local minima on the potential energy surface because their formation is required to create the disulfide bond through a reaction with another neutral or anionic cysteine residue. We found one-step and two-step reaction pathways for the neutral cysteines and two different anionic cysteine pathways. In addition, environmental solvation effects are examined for every calculated transition state. Likely, the most favorable reaction pathway will exhibit the lowest-energy barrier expected to be in the range of 10−20 kcal/mol as typically observed for peroxide oxidation of organic sulfides in an aqueous environment.[50−54]

3.3. High pK_a Neutral Cysteine. In this section, we study in detail the different transition states and local minima structures on two different potential energy surfaces of peroxide oxidation of two neutral cysteine residues. Since the two cysteine residues are identical, we explored the oxidation reaction mechanism on one PES for one neutral cysteine residue with H_2O_2, which ultimately reacts on another PES with the other neutral cysteine residue, forming a disulfide bridge. Additionally, different numbers of solvent-assisted proton exchanges (SAPE) with explicit quantum water molecules and their effect on the different TS activation barriers were examined.

3.3.1. Cysteine Sulfoxide Transition State (TS1).

CSH + H2O2 → CSHO + H2O (1)

We first studied the sulfoxide transition state[31,55] on the M1 model of a neutral cysteine and hydrogen peroxide with zero to two solvent-assisted proton exchanges. All calculated transition states share the same previously reported[35,56] linear arrangement of the sulfur atom, the proximal oxygen (O_p), and the distal oxygen (O_d) atoms of H_2O_2. The transition-state TS1/PE0−PE2 has either a linear, a triangular, or a quadrilateral distribution of the oxygen atoms of H_2O_2 and the water molecules. In the TS1 transition state, breakage of the O_p−O_d bond of H_2O_2 occurs, followed by a transfer of the O_p atom that binds to the sulfur atom of the sulfhydryl group forming a sulfoxide group, while the rest of the H_2O_2 molecule forms a water molecule. We calculated different SAPE transition states that have up to two-proton exchanges with other water molecules.

In TS1/PE0 (Figure S4A), the negatively charged electrophilic proximal oxygen of H_2O_2 attacks the sulfur atom of the sulfhydryl group, which also carries a negative charge (but is much less electronegative). The subsequent reaction evolution involves two consecutive charge distributions upon partial breakage of the O_d−O_p bond (1.88 Å compared to 1.42 Å in RC1) and the approaching of O_p to the sulfur atom (2.04 Å compared to 2.59 Å in RC1). Charge density transfers from the sulfur atom to the O_p atom and finally to the O_d atom: the atomic charge of S changes from −0.33 in RC1 to −0.053 in the TS, O_d changes from −0.32 in RC1 to −0.73 in the TS, while the O_p atomic charge does not change significantly and thus it acts as a hub between the sulfur and the O_d atoms. The

https://dx.doi.org/10.1021/acs.jpcb.0c07510
J. Phys. Chem. B XXXX, XXX, XXX−XXX

Table 2. Thermodynamic Results of the Different Transition States (TS1−TS4) and (TS3-, TS3-*/TS4-, and TS4-*) for the Neutral and the Ionic Cysteines, Respectively[a]

		ΔE_{ZPE}	$\Delta H^{\ddagger}$	$\Delta G^{\ddagger}$	ΔE_{ZPE}	$\Delta H^{\ddagger}$	$\Delta G^{\ddagger}$	ΔE_{ZPE}	$\Delta H^{\ddagger}$	$\Delta G^{\ddagger}$	ΔE_{ZPE}	$\Delta H^{\ddagger}$	$\Delta G^{\ddagger}$
neutral	TS/PE	TS1	TS2	TS3	TS4								
	PE0	60.9	57.8	57.6	43.9	41.1	41.2	68.6	64.6	67.1	143.6	139.2	140.2
	PE1	37.8	35.6	37.3	25.1	22.5	22.4	50.9	48.1	48.9	90.2	85.9	87.9
	PE2	29.4	27.8	30.6	14.9	10.1	12.3	33.0	30.4	32.9	15.7	12.5	15.4
ionic	TS	TS3-/PT1	TS4-/PT1	TS3-*/PE2	TS4-*/PE−PT								
	PT1/PE2/ PE−PT	18.3	17.2	18.2	37.9	33.5	33.8	18.7 (28.5)	17.7 (26.9)	18.6 (27.1)	43.8	41.1	42.0

[a]Values in parenthesis are the thermodynamics results for the *cis*-conformation.

energy penalty for having such O_d-O_p and $S-O_p$ charge separations at the transition state leads to a large Gibbs free-energy activation barrier of 57.6 kcal/mol (Figure S17 and Table 2). In TS1/PE0, no proton exchange occurs but rather an internal proton transfers from the O_p atom to the O_d atom, forming a water molecule in the cysteine sulfoxide intermediate complex (INT1, Figure 1).

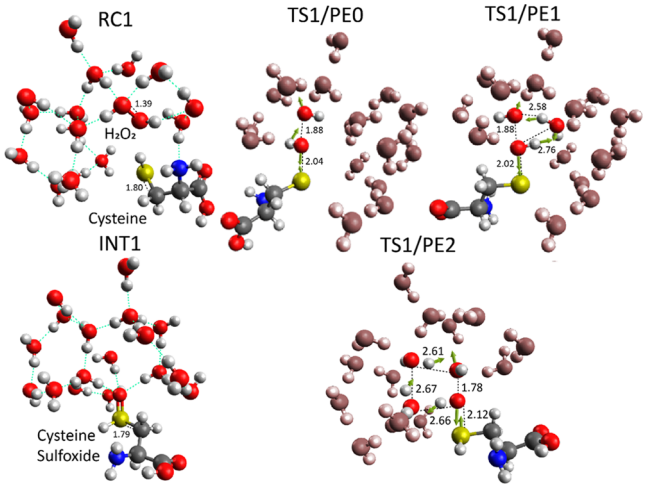

Figure 1. Different SAPE transition states for the first transition state (TS1) with its corresponding reactant complex (RC1) and intermediate complex (INT1), where the hydrogen bonding network is shown as the dashed blue lines. Distances in Angstrom between heavy atoms are shown next to their corresponding dashed lines. For each transition state, QM waters that are not involved in proton exchange are gray-scale colored for clarity. Imaginary frequency eigenvectors are shown for each transition state as the 3D green arrows.

Successive addition of QM waters that are chemically involved in the proton-exchange process noticeably decreases that activation barrier in a monotonic convergent fashion: the first QM water decreases the activation barrier by 20.3 kcal/mol, while the second one decreases it by 6.7 kcal/mol (Figure S17 and Table 2). TS1/PE1 (Figure S4B) QM water exerts its dramatic effect on the activation barrier by stabilizing the charge distribution on the O_p and O_d atoms through a one-proton-exchange process, which leads to a lower energy penalty for the O_d-O_p charge separation at the transition state. Even though the addition of the QM water shifts the charge distribution back to the sulfur atom yet its stabilizing contribution for the major O_d-O_p charge separation outweighs such an increase in the minor $S-O_p$ charge separation, leading to an ultimate decrease of the activation barrier by ∼20 kcal/mol.

Introducing an additional QM water molecule in TS1/PE2 (Figure S4C) with two sets of proton exchanges pushes the O_p-O_d distance by 0.1 Å, increasing the energy penalty of that charge separation. On the other hand, the stabilization effect of two-proton exchanges on the O_p-O_d charge separation and the charge redistribution of O_d clearly outweigh such an energy penalty with an additional decrease of the activation barrier by ∼7 kcal/mol. Proceeding down the energy barrier toward the product complex, the sulfur atom acquires a positive charge of + 0.21, while the newly bonded O_p has a charge of −0.49 in an exergonic reaction with ΔG_R = −36.6 kcal/mol (Figure 9).

The imaginary vibrational frequency vectors for all transition states (TS1/PE0−PE2) demonstrate that their corresponding characteristic vibrational mode involves simultaneous oxygen and proton transfers. Such simultaneous transfers further support the importance of the proton-exchange process in stabilizing the different transition states. Proton exchanges for TS1/PE1−PE2 occur downhill at the corresponding transition state and hence are barrierless.

3.3.2. Cysteine Sulfoxide-to-Sulfenic Acid Tautomer Transition State (TS2).

$$CSHO \rightarrow CSOH \quad (2)$$

Moving forward from the local minimum of the cysteine sulfoxide intermediate complex (INT1) to the local minimum of its tautomer, the cysteine sulfenic acid intermediate complex (INT2), a first-order stationary point was discovered along the reaction pathway on the corresponding potential energy surface. Like TS1, various SAPE transition states were explored, which show a linear, a triangular, or a quadrilateral arrangement (Figure 2). In the TS2 transition state, breakage of the S−H bond of the sulfoxide group occurs, followed by a proton transfer to the oxygen atom of the sulfoxide group, forming a sulfenic acid group. We found that such a tautomerization transition state can occur with or without solvent-assisted proton exchanges with other water molecules.

In TS2/PE0, a simple internal proton transfer occurs at the transition state between the sulfur and the oxygen atoms of the sulfoxide group. At that transition state (Figure S5A), the S−O distance increases by 0.15 Å compared to the corresponding reactant complex (INT1). Nevertheless, it exhibits the highest strained cyclic configuration[57] (∠H−S−O = 54.8°, ∠S−H−O = 71.7°, and ∠S−O−H = 53.4°) with a large energy penalty that leads to a substantial activation barrier of 41.2 kcal/mol (Figure S17 and Table 2). Adding the first QM water in TS2/PE1 (Figure S5B) alleviates notably that configurational strain (∠O−S−H = ∠H−O−H = ∼85°, ∠S−O−H = 95.5°, and S−H−O = ∠O−H-O = ∼135°) and also stabilizes the S−O

https://dx.doi.org/10.1021/acs.jpcb.0c07510
J. Phys. Chem. B XXXX, XXX, XXX−XXX

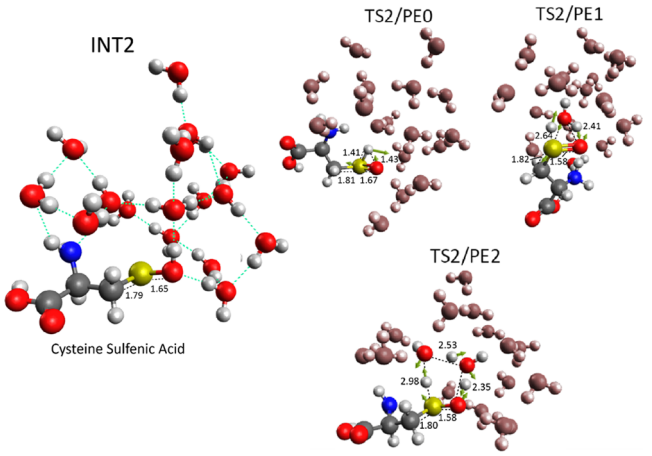

Figure 2. Different SAPE transition states for the second transition state (TS2) with its corresponding intermediate complex (INT2), where the hydrogen bonding network is shown as the dashed blue lines. Distances in Angstrom between the heavy atoms are indicated next to their corresponding dashed lines. For each transition state, QM waters that are not involved in proton exchange are gray-scale colored for clarity. Imaginary frequency eigenvectors are shown for each transition state as the 3D green arrows.

charge separation though a one-proton-exchange process. A decrease in the S−O distance by ∼0.1 Å is observed, but the stabilization effect greatly offsets such an energy penalty with a total reduction in the activation barrier by 18.8 kcal/mol. Subsequent additions of QM waters continuously relieve any remaining configurational strain. In addition, those QM waters stabilize further the S−O charge separation, through a proton-exchange process, with a final decrease in the activation barrier by 10.1 kcal/mol for TS2/PE2 (Figure S5C). Proceeding down the energy barrier to the product complex (INT2), the sulfur atom becomes bonded to an OH group, forming a sulfenic acid group in an exergonic reaction with $\Delta G_R = -19.4$ kcal/mol (Figure 9).

As previously discussed for TS1, the imaginary vibrational frequency vectors for all transition states (TS2/PE1−PE2) show simultaneous oxygen and proton transfers, which further proves the importance of the stabilizing nature of those proton-exchange processes. Unlike TS1, proton exchanges in TS2 show a mixed behavior regarding being either an "uphill" or a "downhill" transfer. For the different transition states (TS2/PE1−PE2), some protons transfer uphill while others transfer downhill. That mixed proton-transfer behavior is due to their different positions and orientations in relieving the configurational strain. For example, in TS2/PE1, the S−H proton transfers downhill, while the water proton transfers uphill. In this fashion, TS2/PE1 ∠H−O−H = 85.3°, while if it was the other way, ∠H−O−H reduces to 64.9°, leading to a higher energy penalty.

3.3.3. Direct Cysteine Sulfenic Acid Transition State (TS3).

$$CSH + H2O2 \rightarrow CSOH + H2O \quad (3)$$

The path from the local minimum of the reactant complex (RC1) to the local minimum of the cysteine sulfenic acid intermediate complex (INT2) can be traversed through a different reaction pathway involving only one first-order saddle point on the corresponding potential energy surface. Like TS1, all calculated transition states show the same linear arrangement formed by the sulfur atom, the proximal oxygen (O_p), and the distal oxygen (O_d) atoms of H_2O_2 for TS3/PE0−PE2 (Figure 3). In that reaction process, the hydrogen peroxide O_p-O_d bond breakage occurs, followed by a transfer of the full HO_p group that bonds to the sulfur atom of the sulfhydryl group. Simultaneously, the S−H bond breaks, and its proton transfers and binds to the HO_d group forming a water molecule. We found that the transition state can occur with or without solvent-assisted proton exchanges with other water molecules.

In TS3/PE0 (Figure S6A), the negatively charged electrophilic proximal oxygen (O_p) of H_2O_2 attacks the sulfur atom of the sulfhydryl group. Similar to TS1, the reaction evolution involves two consecutive charge distributions upon partial breakage of the O_d-O_p bond and the approaching of the O_p atom to the sulfur atom. Charge transfers first from the sulfur atom to the O_p atom, then to the O_d atom: charge of the sulfur atom changes from −0.42 in RC1 to −0.32 in TS, the O_d charge changes from −0.43 in RC1 to −0.64 in TS, and the O_p charge changes from −0.39 in RC1 to −0.11 in TS. Unlike TS1, the sulfur atom carries a larger atomic charge (−0.32 in TS3/PE0 compared to −0.053 in TS1/PE0) due to the proton transfer of the sulfhydryl group. Hence, energy penalties for having both O_d-O_p and $S-O_p$ charge separations (cf. TS1 charge separations) at the transition state contribute significantly toward the high free Gibbs energy activation barrier of 67.08 kcal/mol. Like TS1/PE0, no proton exchange occurs but rather an internal proton transfers from the sulfur to O_d atoms, forming a water molecule in the cysteine sulfenic acid intermediate complex (INT2, Figure S6).

Successive additions of QM water molecules that are chemically involved in the proton-exchange process noticeably decrease the activation barrier in a monotonic fashion: first

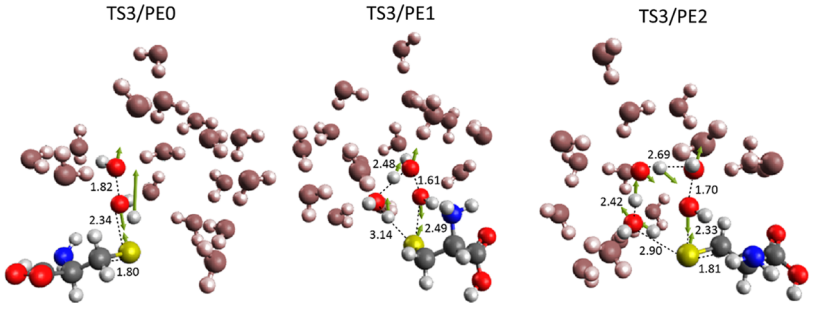

Figure 3. Different SAPE transition states for the third transition state (TS3). Distances in Angstrom between the heavy atoms are indicated next to their corresponding dashed lines. For each transition state, QM waters that are not involved in proton exchange are gray-scale colored. Imaginary frequency eigenvectors are shown for each transition state as the 3D green arrows.

https://dx.doi.org/10.1021/acs.jpcb.0c07510
J. Phys. Chem. B XXXX, XXX, XXX−XXX

QM water decreases the activation barrier by 18.2 kcal/mol, while the second one decreases it by 16.0 kcal/mol (Figure S17 and Table 2). TS3/PE1 (Figure S6B) QM water shows a moderate effect on the activation barrier by stabilizing the charge densities on the sulfur and the O_d atoms through a one-proton-exchange process. This stabilization effect lowers the energy penalties for both the S−O_p and the O_d−O_p charge separations at the transition state. Also, the QM water shifts the charge distribution back to the sulfur atom (atomic charge = −0.76 compared to −0.32 in PE0), and also, the O_d−O_p distance diminishes by 0.22 Å compared to PE0. However, the stabilizing effect of the QM water for both charge separations outweighs those energetic contributions and decreases the activation barrier by ∼18 kcal/mol.

Introducing an additional QM water in TS3/PE2 (Figure S6C) with two sets of proton exchanges relaxes the O_p−O_d distance by 0.1 Å and thus lowering the energy penalty of the O_p−O_d charge separation. More importantly, the stabilization effect of two-proton exchanges on S−O_d charge separation significantly outweighs the energy penalty due to an increase of the O_p charge density, leading to an additional decrease of the activation barrier by 16.0 kcal/mol.

Since at least two bonds break in TS3 (namely, the O_p−O_d and S−H bonds), we examined the highest occupied molecular orbital (HOMO) and HOMO − 1 for TS3/PE0 and TS3/PE2 (Figures S11 and S12, respectively). The TS3/PE0 HOMO and HOMO − 1 clearly show that their electron density mainly spreads over only the sulfhydryl group and the H_2O_2 molecule with no overlap with the orbitals of the neighboring water molecules. On the other hand, the TS3/PE2 HOMO and HOMO − 1 have significant overlap between the orbitals of the sulfhydryl group, the H_2O_2, and the other two water molecules involved in proton exchange. Electron delocalization over larger space—spanning the sulfhydryl group, the H_2O_2 molecule, and the two H_2O molecules—is primarily the stabilization source for the S−O_p and O_d−O_p charge separations imparted by those two water molecules through proton exchanges. Proceeding down the energy barrier to the product complex (Figure S7), the sulfur atom acquires a small negative charge of −0.09, while the newly bonded O_p in the -OH group has a charge of −0.5 in an exergonic reaction with ΔG_R = −55.97 kcal/mol (Figure 9) in a good agreement with the previously reported results.[31]

As discussed above for TS1 and TS2, the imaginary vibrational frequency vectors for all transition states (TS3/PE0−PE2) also demonstrate that their characteristic vibrational modes involve simultaneous oxygen and proton transfers, which further support the importance of such proton exchanges in stabilizing the different transition states. Proton exchanges for TS3/PE1 transfer uphill but move downhill for TS3/PE2 and hence are barrierless (Figure S7). On the other hand, the sulfhydryl proton transfer is always uphill for all transition states TS3/PE0−PE2.

3.3.4. Disulfide Bond Formation Transition State (TS4).

$$\mathrm{CSOH + CSH \rightarrow CSSC + H2O} \quad (4)$$

Indeed, the ultimate goal of the cross-linking reaction is to form a disulfide bond between the cysteine sulfenic acid intermediate and another neutral cysteine residue through a reaction pathway on a higher-dimensional PES. In that bond formation process (Figure 4), breakage of the cysteine sulfenic acid S−OH and the cysteine sulfhydryl S−H bonds occurs, followed by a condensation of the dissociated OH group with

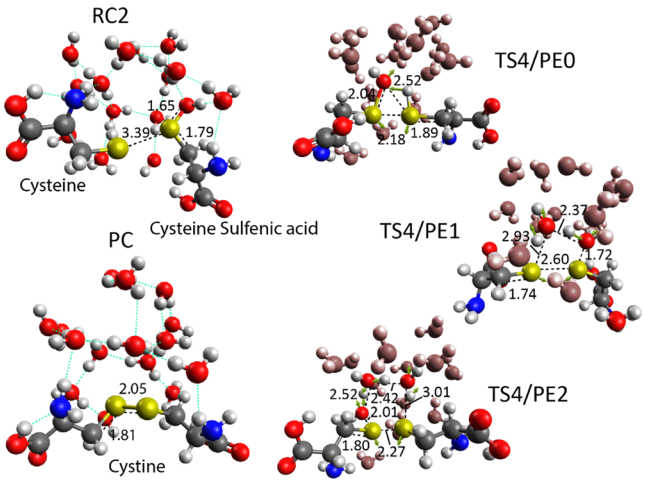

Figure 4. Different SAPE transition states for the fourth transition state (TS4) with its reactant complex (RC2) and product complex (PC), where the hydrogen bonding network is shown as the dashed blue lines. Distances in Angstrom between the heavy atoms are indicated next to their corresponding dashed lines. For each transition state, QM waters that are not involved in proton exchange are gray-scale colored for clarity. Imaginary frequency eigenvectors are shown for each transition state as the 3D green arrows.

the sulfhydryl proton forming a water molecule and a disulfide bond bridging the two sulfur atoms. Such a reaction step can also proceed with or without proton exchange from the other neighboring water molecules.

In TS4/PE0 (Figure S8A), the negatively charged oxygen atom of the sulfenic acid group in the reactant complex (RC2) attacks the positively charged hydrogen atom of the sulfhydryl group. Similar to the previously discussed transition states, reaction evolution involves two charge distributions. Two charge transfers occur in opposite directions upon the partial breakage of both the S−OH bond and the S−H bond and the approach of both the OH group to the hydrogen atom and the two sulfur atoms to each other. One charge transfer happens from the sulfur atom (S_1) of the sulfenic acid group to the bonded oxygen atom, while the second charge transfer occurs from the sulfhydryl proton down to the bonded sulfur atom (S_2). Those charge transfers ultimately lead to a large energy penalty at the transition state, mainly due to multiple charge separations of S_1−O, O−H, H−S_2, and S_1−S_2. All of those charge separations contribute significantly to the large Gibbs free-energy activation barrier of 140.17 kcal/mol. No proton exchange occurs at this transition state, but rather a direct condensation reaction occurs, forming a water molecule and a disulfide bond in the cysteine product complex (PC, Figure S8).

The addition of QM water molecules to TS4/PE0, which are chemically involved in the proton-exchange process, noticeably decreases that activation barrier in a monotonic fashion: the first QM water decreases the activation barrier by 52.27 kcal/mol, while the second one decreases it by 72.49 kcal/mol (Figure S17 and Table 2). The TS4/PE1 (Figure S8B) QM water shows a dramatic effect on the activation barrier by stabilizing the charge separations of S_1−O, S_1−S_2, and other charge separations. The QM water shifts the charge distribution from the S_2 to the S_1 atom and increases the S_1−S_2 distance by 0.42 Å, but the stabilization of the TS charge separations through the one-proton exchange outweighs any

https://dx.doi.org/10.1021/acs.jpcb.0c07510
J. Phys. Chem. B XXXX, XXX, XXX−XXX

unfavorable energetic contributions and thus decrease the activation barrier by ∼52 kcal/mol.

An addition of one more QM water in TS4/PE2 (Figure S8C) with two sets of proton exchanges pushes back the O_p−O_d distance by 0.33 Å, increasing its energy penalty. Nevertheless, the charge redistribution of the S_1 atom and the S_2 atom and the stabilization effect of two-proton exchanges on both the S_1−O and the S_1−S_2 charge separations significantly outweigh the TS energy penalty. Those stabilization effects lead to an additional decrease of the activation barrier by ∼72 kcal/mol to reach a value of 15.4 kcal/mol in close agreement with the reported value of 12.5 kcal/mol by Bayse[58] (which is calculated with four-proton exchanges).

Since at least two bonds break in TS4 (namely, the S_1−OH and the S_2−H bonds), we examined the HOMO and the HOMO − 1 for TS4/PE0 and TS4/PE2 (Figures S13 and S14, respectively). The TS4/PE0 HOMO and HOMO − 1 show that the electron density mainly spreads only over the sulfhydryl and the sulfenic acid groups with negligible orbital overlap with the neighboring water molecules. On the other hand, the TS4/PE2 HOMO and HOMO − 1 have a significant overlap between the orbitals of the sulfhydryl group, the sulfenic acid group, and the two water molecules involved in proton exchange. Like in TS3, electron delocalization over larger space spanning −SOH, −SH, and the two H_2O molecules is primarily the source of the stabilization for the S_1−S_2 and S_1−O charge separations imparted by those two water molecules through proton exchanges. Proceeding down the energy barrier to the product complex, both bridged sulfur atoms acquire negative charges in another exergonic reaction with ΔG_R = −21.23 kcal/mol (Figure 9) in a good agreement with other reported results.[58]

As previously discussed, the imaginary vibrational frequency eigenvectors for all transition states (TS4/PE0−PE2) demonstrate that the characteristic vibrational modes involve simultaneous oxygen and proton transfer, which further supports the importance of proton exchanges in stabilizing the transition state. The proton transfers for PE1−PE2 are mainly downhill and hence are barrierless.

3.4. Low pK_a Ionic Cysteine. In this section, we study in detail the different transition states and local minima structures on two potential energy surfaces of the peroxide oxidation of anionic cysteine residues. Since the two cysteine residues are identical, we explored the oxidation reaction mechanism on one PES for one anionic cysteine residue with H_2O_2, which ultimately reacts on another PES with the other neutral/anionic cysteine residue, forming a disulfide bridge. Unlike the neutral case, both proton transfer (PT) and proton exchanges (PE) were observed. Based on our previous calculations, we only studied the anionic transition states (TS3-* and TS4-*) with two-proton exchanges or proton exchange−proton transfer, as we found previously that two-proton exchanges provide enough TS stabilization.

3.4.1. Direct Cysteine Sulfenic Acid Transition State (TS3-).

$$CS^- + H2O2 \rightarrow CSOH + HO^- \quad (5)$$

Another possibility to reach the local minimum of the cysteine sulfenic acid intermediate is through a reaction between a H_2O_2 and an anionic cysteine residue (RC1-). This reaction mechanism represents the first step in reaction scheme I of Luo et al.,[54] where the nucleophilic thiolate group attacks the proximal oxygen of H_2O_2. Such a reaction pathway occurs on a close lower-dimensional PES to the neutral case (TS3) and leads to a production of the intermediate complex of a cysteine sulfenic acid and a hydroxyl anion (INT2-).

Similar to the neutral case of TS3, the calculated transition state shows a linear arrangement of the sulfur atom, the proximal oxygen (O_p), and the distal oxygen (O_d) atoms of H_2O_2 (Figure 5). In the current reaction mechanism, a

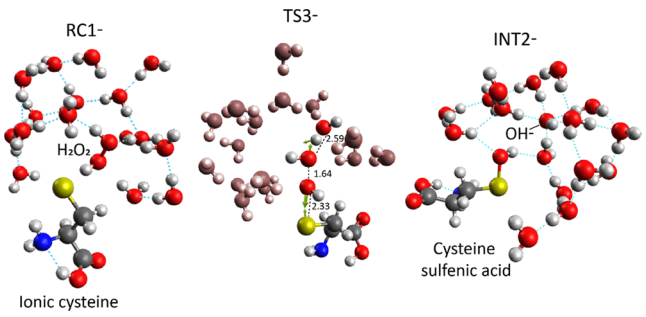

Figure 5. Ionic direct cysteine sulfenic acid transition state (TS3-) with its corresponding reactant complexes (RC1-) and intermediate complex (INT2-), where the hydrogen bonding network is shown as the dashed blue lines. Distances in Angstrom are indicated next to their corresponding dashed lines. For the transition state, QM waters that are not involved in proton transfer are gray-scale colored for clarity. Imaginary frequency eigenvectors are shown for each transition state as the 3D green arrows.

breakage of the hydrogen peroxide O_p−O_d bond occurs, followed by a transfer of the full HO_p group to the sulfur atom of the thiolate group. Simultaneously, a proton transfers from a nearby water molecule to the HO_d group, producing a water molecule and a hydroxyl (OH−) group.

As in the neutral case of TS3, the reaction evolution in TS3- involves two consecutive charge distributions. Upon partial breakage of the O_d−O_p bond and the approach of the O_p atom toward the sulfur atom, the charge density transfers from the sulfur atom to the O_p atom and then to the O_d atom (Figure S6D). The O_d atom carries the largest charge density at the transition state, and therefore, the O_d−O_p charge separation contributes the most toward the TS energy penalty. Solvent-assisted proton transfer (SAPT) from a hydrogen-bonded water molecule to the HO_d group significantly stabilizes the O_d−O_p charge separation through delocalizing their electron population over a larger space (Figure S15). Furthermore, three water molecules stabilize the newly formed OH− group through hydrogen bonding, which collectively leads to a significant drop of the activation barrier to 18.2 kcal/mol in close agreement with experimental[54] and other theoretical[33] results. We anticipate that having a water molecule under low pH conditions as the leaving group (the OH− group and H+) would significantly lower the activation barrier. Similarly, as other transition states, the imaginary vibrational frequency mode proves simultaneous oxygen and proton transfer, which supports the importance of such proton transfer in stabilizing the transition state.

3.4.2. Cysteine Sulfenate Anion Transition State (TS3-/PE2).*

$$CS^- + H2O2 \rightarrow CSO^- + H2O \quad (6)$$

Another essential intermediate complex is the deprotonated cysteine sulfenic acid, reported previously by many authors.[35,59] On a similar PES to TS3-, this reaction mechanism also occurs between a H_2O_2 and an anionic cysteine residue (RC1-/RC1-*), producing the intermediate complex of a

https://dx.doi.org/10.1021/acs.jpcb.0c07510
J. Phys. Chem. B XXXX, XXX, XXX−XXX

cysteine sulfenate anion and a water molecule (INT2-*) instead. The TS3-* transition state also shows a linear arrangement of the sulfur atom, the proximal oxygen (O_p), and the distal oxygen (O_d) atoms of H_2O_2 (Figure 6). In the current reaction mechanism, a breakage of the hydrogen peroxide O_p-O_d bond occurs, followed by a transfer of the O_p atom to the sulfur atom of the thiolate group. Simultaneously, two-proton exchanges occur between the HO_p proton, two water molecules, and the HO_d group, which forms a water molecule.

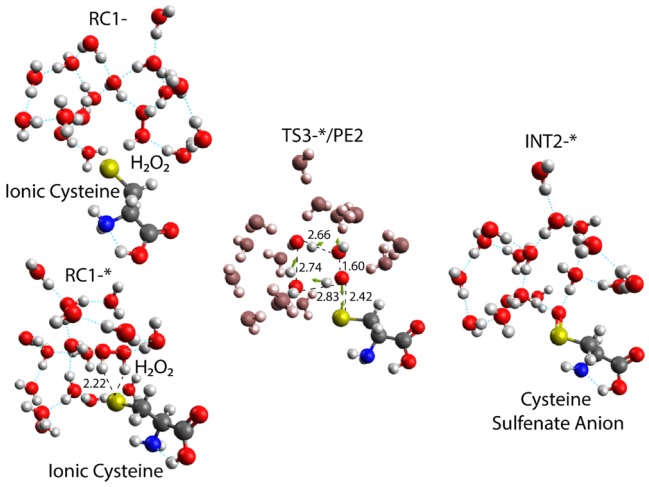

Figure 6. Cysteine sulfenate anion transition state (TS3-*) with its corresponding reactant complexes (RC1-/RC1-*) and intermediate complex (INT2-*), where the hydrogen bonding network is shown as the dashed blue lines. Distances in Angstrom are indicated next to their corresponding dashed lines. For the transition state, QM waters that are not involved in proton exchange are gray-scale colored for clarity. Imaginary frequency eigenvectors are shown for the transition state as the 3D green arrows.

In contrast with the previously calculated transition states, the reaction evolution in TS3-*/PE2 does not show significant charge rearrangement as clearly indicated by the constant atomic charge (∼−0.8) of the thiolate sulfur atom and the H_2O_2 oxygen atoms (∼−0.35 and ∼−0.5) at TS compared to RC1-/RC1-* (Figure S9). Previous experimental reports also suggest that no significant charge redistribution occurs at the transition state,[60] which explains the pH-independence of the oxidation rate constants.[35]

Since we found that two-proton exchanges provide enough stabilization effect, we only studied the current transition state with two-proton exchanges. Unlike TS3-, two reactant complexes (RC1-/RC1-*) were found where the H_2O_2 has either a *skew*-conformation (RC1-) with an activation barrier of 18.6 kcal/mol in close agreement with experimental[54] and other theoretical[35] results or a *cis*-conformation with a higher activation barrier of 27.1 kcal/mol (Table 2 and Figure 10). Proceeding down the energy barrier to the product complex, the cysteine sulfenate ion intermediate complex (INT2-*) is formed in an exergonic reaction with $\Delta G_R \sim -47$ kcal/mol (Figure 10). Due to the lower pK_a value of the cysteine sulfenic acid compared to water, INT2-* is found to be thermodynamically more stable than INT2- by 27.8 kcal/mol. Similarly, as other transition states, the imaginary vibrational frequency mode proves simultaneous oxygen and proton transfer, which supports the importance of such proton transfers in stabilizing the transition state.

3.4.3. Ionic Disulfide Cross-Linking Transition State through Cysteine Sulfenic Acid (TS4-).

$$CS^- + CSOH \rightarrow CSSC + HO^- \quad (7)$$

An alternative reaction pathway to form a disulfide bridge is through a reaction between the cysteine sulfenic acid and an anionic cysteine residue (RC2-), similar to the second step in reaction scheme I of Luo et al.[54] Such a reaction takes place on a similar but lower-dimensional PES of the neutral case (TS4) and leads to a production of the cystine molecule and hydroxyl ion product complex (PC-) (Figure 7).

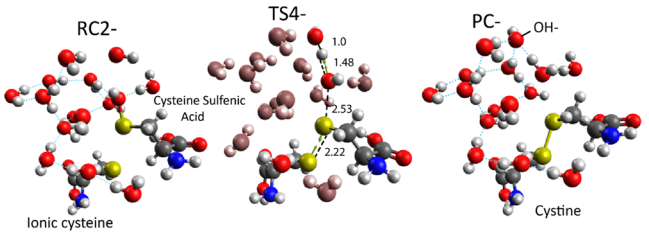

Figure 7. Ionic transition state of the disulfide bond formation (TS4-) with its corresponding reactant complex (RC2-) and product complex (PC-), where the hydrogen bonding network is shown as the dashed blue lines. Distances in Angstrom are indicated next to their corresponding dashed lines. For the transition state, QM waters that are not involved in proton transfer are gray-scale colored for clarity. Imaginary frequency eigenvectors are shown for each transition state as the 3D green arrows.

Due to the nucleophilic attack of the thiolate group on the backside of the −SOH group, the calculated transition state shows a nearly linear arrangement of the two sulfur atoms and the oxygen atom of the sulfenic acid group (Figure 7). In the current nucleophilic substitution reaction, the sulfenic acid S−OH bond partially breaks, and a partial formation of the disulfide bond occurs. Simultaneously, the O−H bond of a neighboring water molecule breaks, and a proton transfer occurs, producing a water molecule and a OH− group.

Like previous transition states, the reaction evolution in TS4- involves two consecutive charge distributions. Upon partial breakage of the S−OH bond and approach of the two sulfur atoms, charge density transfers from the sulfur atom of the S−OH group to its oxygen atom and finally to the oxygen atom of the water molecule. Two charge separations exist in TS4-, namely, the S_1-S_2 and S_1-O charge separations, where all atoms carry negative charges (Figure S8D). Additionally, we inspected the HOMO (which is mainly centered on the thiolate group) and the lowest unoccupied molecular orbital (LUMO) of the cysteine sulfenic acid (which is mainly characterized by the S−O σ^* bond) (Figure S16), which show a significant out-of-phase overlap in the region between the two sulfur atoms. Collectively, the TS charge separations and the significant destructive interference lead to a high Gibbs free-energy activation barrier of 33.8 kcal/mol. Like TS3-, under acidic conditions, the poor leaving OH− group would form a good leaving water molecule that is expected to have a lower activation barrier. Proceeding down the energy barrier to the product complex, the disulfide bond is formed in an endergonic reaction with $\Delta G_R = +24.3$ kcal/mol (Figure 10) as expected for a weak leaving OH− group in a nucleophilic substitution reaction.[61]

https://dx.doi.org/10.1021/acs.jpcb.0c07510
J. Phys. Chem. B XXXX, XXX, XXX−XXX

3.4.4. Ionic Disulfide Cross-Linking Transition State through Cysteine Sulfenate Anion (TS4-/PE2).*

$$CSO^- + CSH \rightarrow CSSC + HO^- \quad (8)$$

Another possibility to form the disulfide bridge is through the reaction between the cysteine sulfenate anion and a neutral cysteine residue (RC2-*, Figure 8). This reaction occurs on a similar PES to TS4- and leads the product complex (PC-) of a cystine molecule and a hydroxyl ion. Due to the strong acidic character of the cysteine sulfenic acid compared to the neutral cysteine,[62,63] RC2-* was found to be thermodynamically more stable than RC2- by 36.7 kcal/mol.

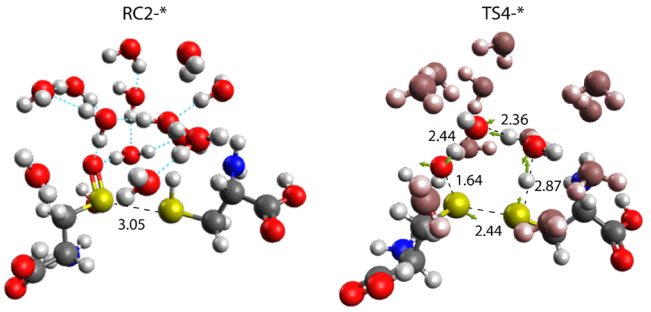

Figure 8. Ionic transition state of the disulfide bond formation (TS4-*) with its corresponding reactant complex (RC2-*), where the hydrogen bonding network is shown as the dashed blue lines. Distances in Angstrom are indicated next to their corresponding dashed lines. For the transition state, QM waters that are not involved in proton transfer are gray-scale colored for clarity. Imaginary frequency eigenvectors are shown for each transition state as the 3D green arrows.

In the current reaction, the sulfenate S−O and the thiol S−H bonds partially break, and a partial formation of the disulfide bond occurs. Simultaneously, the O−H bonds of two water molecules partially break, and proton exchange−proton transfer (PE−PT) occurs, producing a cystine molecule and a OH− group. Similar to TS4, multiple charge separations exist between the two sulfur atoms, S−O, and two O−O charge separations (Figure S10). Although PE−PT stabilizes TS4-*/PE2 (cf. TS4/PE2), the extra-negative charge of the sulfenate anion and the nature of the poor leaving group of OH− (in a quasi-nucleophilic substitution reaction) raise the TS energy penalties and so lead to a high Gibbs free-energy activation barrier of 42.0 kcal/mol (Table 2 and Figure 10).

3.5. Overall Mechanism of the Disulfide Cross-Linking Reaction. Inspecting the energy barriers for the different calculated transition states (Figure S17) shows conspicuously that those barriers are insurmountable without explicit water contributions through either proton exchange, proton transfer, or hydrogen bonding. Electron delocalization at the transition state is the primary source of stabilization provided by those chemically involved water molecules through proton-exchange or proton-transfer processes. Electron delocalization over larger space stabilizes the different charge separations at the transition state, which lowers their energetic penalties toward the activation barrier. Some of the calculated transition states have substantial activation barriers and hence are unfeasible under normal conditions but might be favorable (with lower barriers) under different conditions. Besides, we included those transition states to provide a comprehensive reference for the various reaction pathways of the disulfide cross-linking reaction with hydrogen peroxide.

For the neutral case (Figure 9), since water molecules stabilize the S−O_d charge separation at TS3 and the O_p−O_d charge separation at TS1, it is energetically comparable to proceed through either the one-step reaction pathway or the two-step pathway by ∼2.0 kcal/mol. Formation of the cysteine sulfenic acid intermediate through either TS1 or TS3 is higher than the disulfide bond formation step through TS4 by ∼15.0 kcal/mol. So the formation of the cysteine sulfenic acid represents the rate-determining step, as previously reported.[64] The larger stability of TS4 can be explained by the larger electron delocalization over the two partially bonded sulfur atoms at the transition state.

For the ionic case (Figure 10), TS3- is the only accessible transition state for the formation of the cysteine sulfenic acid intermediate. The reaction barrier of TS3- is lower by ∼14 kcal/mol compared to TS3 in the neutral case, which is primarily due to a larger electron delocalization of the negatively charged thiolate group. That would explain the higher reaction rates of free cysteines with hydrogen peroxide at alkaline pH,[65] where it dissociates to anionic cysteines. Other studies also reported lower barriers in general for the

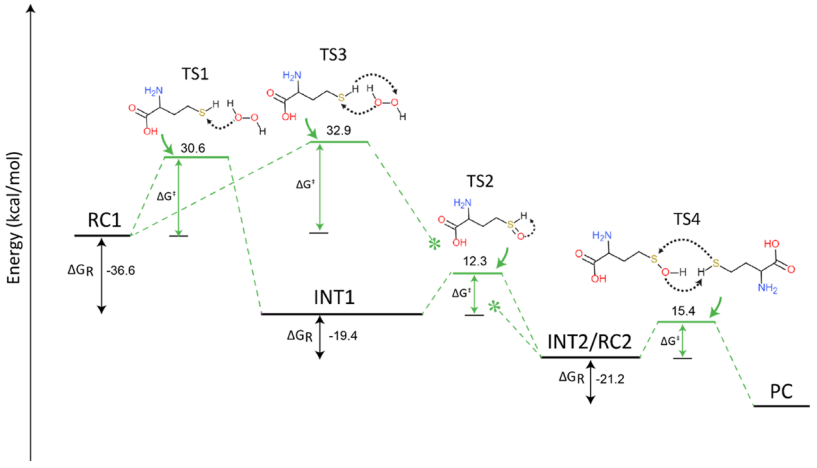

Figure 9. Lowest Gibbs free-energy activation barriers (with two-proton exchanges) and reaction energies for the different transition states and local minima structures in the disulfide cross-linking reaction for the neutral cysteine case (TS3 connecting the dashed lines was truncated for clarity). Schematic TS representation is shown above its corresponding TS.

https://dx.doi.org/10.1021/acs.jpcb.0c07510
J. Phys. Chem. B XXXX, XXX, XXX−XXX

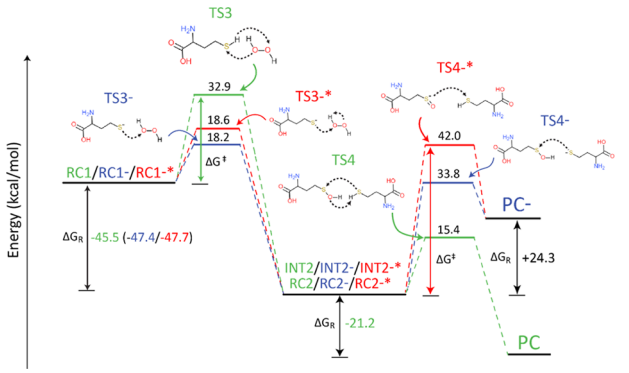

Figure 10. Gibbs free-energy barriers and reaction energies for the neutral TS3/TS4 (shown in green) versus the ionic TS3-/TS4- (shown in blue) and TS3-*/TS4-* (shown in red). Values in parenthesis are ΔG_R for the ionic case. Schematic TS representation is shown next to its corresponding TS.

anionic methanethiolate compared to the methanethiol models.[31] However, a particular stabilization effect of the surrounding microenvironment could make TS3 the favorable reaction pathway compared to TS3-. Unlike the neutral case, the formation of the cysteine sulfenic acid intermediate through TS3- is not the rate-limiting step compared to the disulfide bond formation step through TS4-, which is higher by ∼15 kcal/mol. Additionally, the energy barrier for TS4- is higher than that of TS4 by ∼18 kcal/mol, which is mainly due to the nature of the poor leaving group of OH− in TS4- compared to the good leaving water molecule in TS4.

In addition, the production of cysteine sulfenate anion through TS3-* is another possible reaction pathway toward the disulfide bond formation. Similar to TS3-, TS3-* is not the rate-limiting step compared to TS4-*, which is significantly elevated (Figure 10) due to the energetically unfavorable negative charge of the sulfenate S−O group and the poor nature of the OH− leaving group in a quasi-nucleophilic substitution reaction.

To sum up, in the current study, we explored various transition states and local minima structures over different potential energy surfaces for the disulfide cross-linking reaction (Figure S17). For the case of neutral cysteines, the formation of the cysteine sulfoxide (TS1/PE2 in reaction 1, Figure S18) is found to be the rate-limiting step and yet very comparable in its Gibbs free-energy activation barrier to that of the direct cysteine sulfenic acid transition state (TS3/PE2 in reaction 3). Similarly, in the ionic case, the Gibbs free-energy activation barriers for both the cysteine sulfenic acid (TS3- in reaction 5) and the cysteine sulfenate ion (TS3-* in reaction 6) are almost identical. The reaction pathways for the neutral case are either a two-step tautomeric process (reactions 1 = >2), which passes over the intermediate cysteine sulfoxide or a one-step direct process (reaction 3), which goes directly to the cysteine sulfenic acid intermediate, as for the case of the anionic system (reaction 5). Also, the anionic system can form instead of the deprotonated form of the cysteine sulfenic acid (reaction 6). Eventually, the cysteine sulfenic acid or the cysteine sulfenate anion reacts with another neutral cysteine (reactions 4 and 8) or anionic one (reaction 7) to produce the cystine molecule.

4. CONCLUSIONS

In the current study, a total of 16 different transition states were calculated, at the QM/MM level of theory using PBE50/6-311++G** and Amber03 force field, with their corresponding reactant and product complexes on a model system of a pair of neutral or anionic cysteine residues in a periodic water box. For the neutral cysteine system, 12 transition states were discovered with different numbers of solvent-assisted proton exchanges. Additionally, four transition states were studied for the ionic case with either one SAPT, two SAPE, or SAPE/SAPT. For the neutral case, the cysteine sulfenic acid formation represents the rate-limiting step through either TS1/TS2 or TS3, compared to the disulfide bond formation step through TS4. The ionic case shows an opposite behavior where the Gibbs free-energy barriers of the cysteine sulfenic acid TS3- or the cysteine sulfenate ion TS3-* are much lower than those of the disulfide bond formation step through either TS4- or TS4-*, which represents the rate-limiting step. It is worth noting that the formation of the disulfide bond through TS4 represents the most favorable exergonic reaction pathway compared to either TS4- or TS4-* endergonic reaction pathways due to mainly the nature of the good leaving water molecule in TS4 in contrast to the poor leaving OH− group in TS4- and TS4-*.

In addition, our results show clearly that explicit water molecules play an essential role in reducing the Gibbs free-energy activation barriers for all calculated transition states. Electron delocalization represents the primary source of stabilization of those water molecules through either SAPE, SAPT, or hydrogen bonding, which reduces the energy penalty of the different charge separations at the transition state. Additionally, those water molecules reduce the energy penalty due to any configurational strain of the transition state.

The QM/MM method with an explicit periodic water box shows a better agreement with experimental results than previous reports. For example, the TS3- free-energy barrier of 18.2 kcal/mol conforms better with the experimental value of 16.96 kcal/mol[54] than 20.7 kcal/mol on a methanethiol model in vacuo[59] or even on a model of cysteine in PCM with a 19.0 kcal/mol activation barrier.[33] Our results also demonstrate that the cysteine sulfenic acid formation is the rate-limiting step (k_1^*) through TS3- rather than the disulfide bond formation step (k_2^*) through TS4. Fitting the calculated activation barriers to the Arrhenius equation shows that $k_2^* \gg k_1^*$ by 1 order of magnitude, which is quantitively close to other experimental studies,[54,64] which show that $k_2 \gg k_1$ by about 38 times at 298 K and over pH 4−13.

■ ASSOCIATED CONTENT

Supporting Information

The Supporting Information is available free of charge at https://pubs.acs.org/doi/10.1021/acs.jpcb.0c07510.

Benchmarked disulfide bond transition state with its reactant and product complexes (Figure S1); lists the different benchmarked energetic results of the disulfide bond transition state and its reactant complex (Table S1); M1 and M2 models used for the transition-state calculations (Figures S2 and S3); different SAPE/SAPT transition states with their corresponding reactant and product complexes for TS1, TS2, TS3/TS3-/TS3-*, and TS4/TS4-/TS4-* (Figures S4, S5, S6, S8, S9, and S10); reaction evolution of TS3/PE2 (Figure S7); HOMO and HOMO − 1 of TS3/PE0, TS3/PE2, TS4/PE0, TS4/PE2, and TS3-/PT1 (Figures S11−S15); HOMO of ionic cysteine and the LUMO of cysteine sulfenic acid

https://dx.doi.org/10.1021/acs.jpcb.0c07510
J. Phys. Chem. B XXXX, XXX, XXX−XXX

in TS4-/PT1 (Figure S16); Gibbs free-energy activation barriers and reaction energies for the different transition states (TS1−TS4) for the neutral cysteines (Figure S17); overall mechanism of the disulfide cross-linking reaction (Figure S18) (PDF)

AUTHOR INFORMATION

Corresponding Author

Bernhardt L. Trout − *Department of Chemical Engineering, Massachusetts Institute of Technology, Cambridge, Massachusetts 02139, United States;* orcid.org/0000-0003-1417-9470; Email: trout@mit.edu

Authors

Muhammad A. Hagras − *Department of Chemical Engineering, Massachusetts Institute of Technology, Cambridge, Massachusetts 02139, United States;* orcid.org/0000-0002-6062-2544

Michael A. Bellucci − *Department of Chemical Engineering, Massachusetts Institute of Technology, Cambridge, Massachusetts 02139, United States; XtalPi Inc., Cambridge, Massachusetts 02142, United States*

Gianpaolo Gobbo − *Department of Chemical Engineering, Massachusetts Institute of Technology, Cambridge, Massachusetts 02139, United States; XtalPi Inc., Cambridge, Massachusetts 02142, United States;* orcid.org/0000-0002-8294-6152

Ryan A. Marek − *MMD, Merck & Co Inc., West Point, Pennsylvania 19486, United States*

Complete contact information is available at: https://pubs.acs.org/10.1021/acs.jpcb.0c07510

Notes

The authors declare no competing financial interest.

ACKNOWLEDGMENTS

We thank Merck Sharp & Dohme Corp., a subsidiary of Merck & Co., Inc., Kenilworth, NJ, USA, for their financial support of this research.

REFERENCES

(1) Liu, H.; May, K. Disulfide bond structures of IgG molecules. *mAbs* **2012**, *4*, 17−23.

(2) Martinez, T.; Guo, A.; Allen, M. J.; Han, M.; Pace, D.; Jones, J.; Gillespie, R.; Ketchem, R. R.; Zhang, Y.; Balland, A. Disulfide Connectivity of Human Immunoglobulin G2 Structural Isoforms. *Biochemistry* **2008**, *47*, 7496−7508.

(3) McAuley, A.; Jacob, J.; Kolvenbach, C. G.; Westland, K.; Lee, H. J.; Brych, S. R.; Rehder, D.; Kleemann, G. R.; Brems, D. N.; Matsumura, M. Contributions of a disulfide bond to the structure, stability, and dimerization of human IgG1 antibody CH3 domain. *Protein Sci.* **2008**, *17*, 95−106.

(4) Reiter, Y.; Brinkmann, U.; Jung, S.-H.; Pastan, I.; Lee, B. Disulfide stabilization of antibody Fv: computer predictions and experimental evaluation. *Protein Eng., Des. Sel.* **1995**, *8*, 1323−1331.

(5) Wang, W.; Singh, S.; Zeng, D. L.; King, K.; Nema, S. Antibody structure, instability, and formulation. *J. Pharm. Sci.* **2007**, *96*, 1−26.

(6) Sapp, M.; Fligge, C.; Petzak, I.; Harris, J. R.; Streeck, R. E. Papillomavirus Assembly Requires Trimerization of the Major Capsid Protein by Disulfides between Two Highly Conserved Cysteines. *J. Virol.* **1998**, *72*, 6186.

(7) Anfinsen, C. B.; Haber, E.; Sela, M.; White, F. H., Jr The kinetics of formation of native ribonuclease during oxidation of the reduced polypeptide chain. *Proc. Natl. Acad. Sci. U.S.A.* **1961**, *47*, 1309.

(8) Creighton, T. E. [5] Disulfide Bonds as Probes of Protein Folding Pathways. In *Methods in Enzymology*; Elsevier, 1986; Vol. *131*, pp 83−106.

(9) Creighton, T. E. Disulphide bonds and protein stability. *BioEssays* **1988**, *8*, 57−63.

(10) Gilbert, H. F. Protein disulfide isomerase and assisted protein folding. *J. Biol. Chem.* **1997**, *272*, 29399−29402.

(11) Jaenicke, R. Folding and association of proteins. *Prog. Biophys. Mol. Biol.* **1987**, *49*, 117−237.

(12) Jaenicke, R. Protein folding: local structures, domains, subunits, and assemblies. *Biochemistry* **1991**, *30*, 3147−3161.

(13) Long, D.; Cohen, G. H.; Muggeridge, M. I.; Eisenberg, R. J. Cysteine mutants of herpes simplex virus type 1 glycoprotein D exhibit temperature-sensitive properties in structure and function. *J. Virol.* **1990**, *64*, 5542−5552.

(14) Braakman, I.; Helenius, J.; Helenius, A. Manipulating disulfide bond formation and protein folding in the endoplasmic reticulum. *EMBO J.* **1992**, *11*, 1717−1722.

(15) Karnik, S. S.; Sakmar, T. P.; Chen, H.-B.; Khorana, H. G. Cysteine residues 110 and 187 are essential for the formation of correct structure in bovine rhodopsin. *Proc. Natl. Acad. Sci. U.S.A.* **1988**, *85*, 8459−8463.

(16) Ortega, S.; Schaeffer, M.-T.; Soderman, D.; DiSalvo, J.; Linemeyer, D. L.; Gimenez-Gallego, G.; Thomas, K. A. Conversion of cysteine to serine residues alters the activity, stability, and heparin dependence of acidic fibroblast growth factor. *J. Biol. Chem.* **1991**, *266*, 5842−5846.

(17) Suganuma, N.; Matzuk, M. M.; Boime, I. Elimination of disulfide bonds affects assembly and secretion of the human chorionic gonadotropin beta subunit. *J. Biol. Chem.* **1989**, *264*, 19302−19307.

(18) Cabiscol Català, E.; Tamarit Sumalla, J.; Ros Salvador, J. Oxidative stress in bacteria and protein damage by reactive oxygen species. *Int. Microbiol.* **2000**, *3*, 3−8.

(19) Lee, S.-R.; Yang, K.-S.; Kwon, J.; Lee, C.; Jeong, W.; Rhee, S. G. Reversible inactivation of the tumor suppressor PTEN by H2O2. *J. Biol. Chem.* **2002**, *277*, 20336−20342.

(20) Costanzo, J. P.; Lee, R. E., Jr.; DeVries, A. L.; Wang, T.; Layne, J. R., Jr. Survival mechanisms of vertebrate ectotherms at subfreezing temperatures: applications in cryomedicine. *FASEB J.* **1995**, *9*, 351−358.

(21) Bar, M.; Bar-Ziv, R.; Scherf, T.; Fass, D. Efficient production of a folded and functional, highly disulfide-bonded β-helix antifreeze protein in bacteria. *Protein Expression Purif.* **2006**, *48*, 243−252.

(22) Muldrew, K.; Rewcastle, J.; Donnelly, B. J.; Saliken, J. C.; Liang, S.; Goldie, S.; Olson, M.; Baissalov, R.; Sandison, G. Flounder antifreeze peptides increase the efficacy of cryosurgery. *Cryobiology* **2001**, *42*, 182−189.

(23) Lindsay, M. P.; Skerritt, J. H. The glutenin macropolymer of wheat flour doughs: structure−function perspectives. *Trends Food Sci. Technol.* **1999**, *10*, 247−253.

(24) Gerrard, J. A. Protein−protein cross-linking in food: methods, consequences, applications. *Trends Food Sci. Technol.* **2002**, *13*, 391−399.

(25) Zayas, J. F. *Functionality of Proteins in Food*; Springer Science & Business Media, 2012.

(26) Dombkowski, A. A.; Sultana, K. Z.; Craig, D. B. Protein disulfide engineering. *FEBS Lett.* **2014**, *588*, 206−212.

(27) Yue, H.; Bu, X.; Huang, M.-H.; Young, J.; Raglione, T. Quantitative determination of trace levels of hydrogen peroxide in crospovidone and a pharmaceutical product using high performance liquid chromatography with coulometric detection. *Int. J. Pharm.* **2009**, *375*, 33−40.

(28) Huang, T.; Garceau, M. E.; Gao, P. Liquid chromatographic determination of residual hydrogen peroxide in pharmaceutical excipients using platinum and wired enzyme electrodes. *J. Pharm. Biomed. Anal.* **2003**, *31*, 1203−1210.

(29) Crowley, P.; Martini, L. G. Drug-excipient interactions. *Pharm. Technol.* **2001**, *4*, 7−12.

https://dx.doi.org/10.1021/acs.jpcb.0c07510
J. Phys. Chem. B XXXX, XXX, XXX−XXX

(30) Hartauer, K. J.; Arbuthnot, G. N.; Baertschi, S. W.; Johnson, R. A.; Luke, W. D.; Pearson, N. G.; Rickard, E. C.; Tingle, C. A.; Tsang, P. K. S.; Wiens, R. E. Influence of peroxide impurities in povidone and crospovidone on the stability of raloxifene hydrochloride in tablets: identification and control of an oxidative degradation product. *Pharm. Dev. Technol.* **2000**, *5*, 303−310.
(31) van Bergen, L. A. H.; Roos, G.; De Proft, F. From thiol to sulfonic acid: Modeling the oxidation pathway of protein thiols by hydrogen peroxide. *J. Phys. Chem. A* **2014**, *118*, 6078−6084.
(32) Khavani, M.; Izadyar, M.; Reza Housaindokht, M. Quantum chemistry study on the mechanism of oxidation of cysteine to cystine using hydrogen peroxide. *Phosphorus, Sulfur Silicon Relat. Elem.* **2015**, *190*, 1680−1691.
(33) Cardey, B.; Enescu, M. Selenocysteine versus cysteine reactivity: a theoretical study of their oxidation by hydrogen peroxide. *J. Phys. Chem. A* **2007**, *111*, 673−678.
(34) Bayse, C. A. Transition states for cysteine redox processes modeled by DFT and solvent-assisted proton exchange. *Org. Biomol. Chem.* **2011**, *9*, 4748−4751.
(35) Zeida, A.; Babbush, R.; Lebrero, M. C. G.; Trujillo, M.; Radi, R.; Estrin, D. A. Molecular basis of the mechanism of thiol oxidation by hydrogen peroxide in aqueous solution: challenging the SN2 paradigm. *Chem. Res. Toxicol.* **2012**, *25*, 741−746.
(36) Valiev, M.; Bylaska, E. J.; Govind, N.; Kowalski, K.; Straatsma, T. P.; Van Dam, H. J. J.; Wang, D.; Nieplocha, J.; Apra, E.; Windus, T. L.; de Jong, W. A. NWChem: A comprehensive and scalable open-source solution for large scale molecular simulations. *Comput. Phys. Commun.* **2010**, *181*, 1477−1489.
(37) Adamo, C.; Barone, V. Toward reliable density functional methods without adjustable parameters: The PBE0 model. *J. Chem. Phys.* **1999**, *110*, 6158−6170.
(38) Ponder, J. W.; Case, D. A. Force Fields for Protein Simulations. In *Advances in Protein Chemistry*; Elsevier, 2003; Vol. *66*, pp 27−85.
(39) Berendsen, H. J. C.; van der Spoel, D.; van Drunen, R. GROMACS: A message-passing parallel molecular dynamics implementation. *Comput. Phys. Commun.* **1995**, *91*, 43−56.
(40) Zhang, Y.; Liu, H.; Yang, W. Free energy calculation on enzyme reactions with an efficient iterative procedure to determine minimum energy paths on a combined ab initio QM/MM potential energy surface. *J. Chem. Phys.* **2000**, *112*, 3483−3492.
(41) Peverati, R.; Truhlar, D. G. Improving the Accuracy of Hybrid Meta-GGA Density Functionals by Range Separation. *J. Phys. Chem. Lett.* **2011**, *2*, 2810−2817.
(42) Mardirossian, N.; Head-Gordon, M. Characterizing and understanding the remarkably slow basis set convergence of several Minnesota density functionals for intermolecular interaction energies. *J. Chem. Theory Comput.* **2013**, *9*, 4453−4461.
(43) Kortemme, T.; Creighton, T. E. Ionisation of Cysteine Residues at the Termini of Model α-Helical Peptides. Relevance to Unusual Thiol pK_a Values in Proteins of the Thioredoxin Family. *J. Mol. Biol.* **1995**, *253*, 799−812.
(44) Zeida Camacho, A. F.; Guardia, C. M. A.; Lichtig, P.; Perissinotti, L. L.; Defelipe, L. A.; Turjanski, A.; Radi, R.; Trujillo, M.; Estrin, D. A. Thiol redox biochemistry: Insights from computer simulations. *Biophys. Rev.* **2014**, *6*, 27−46.
(45) Roos, G.; Foloppe, N.; Messens, J. Understanding the pK_a of redox cysteines: The key role of hydrogen bonding. *Antioxid. Redox Signaling* **2013**, *18*, 94−127.
(46) *The Merck Index*; Rahway, N. M. C., Ed.; Merck & Co. Inc.: Rahway, NJ, 1989.
(47) Benesch, R. E.; Benesch, R. The acid strength of the-SH group in cysteine and related compounds. *J. Am. Chem. Soc.* **1955**, *77*, 5877−5881.
(48) Marino, S. M.; Gladyshev, V. N. Analysis and functional prediction of reactive cysteine residues. *J. Biol. Chem.* **2012**, *287*, 4419−4425.
(49) Jao, S.-C.; English Ospina, S. M.; Berdis, A. J.; Starke, D. W.; Post, C. B.; Mieyal, J. J. Computational and mutational analysis of human glutaredoxin (thioltransferase): probing the molecular basis of the low p K a of cysteine 22 and its role in catalysis. *Biochemistry* **2006**, *45*, 4785−4796.
(50) Curci, R.; DiPrete, R.; Edwards, J. O.; Modena, G. Role of solvent in the oxidation of some organic compounds by peroxyacids. *J. Org. Chem.* **1970**, *35*, 740−745.
(51) Behrman, E. J.; Edwards, J. O., Nucleophilic Displacements on Peroxide Oxygen and Related Reactions. In *Progress in Physical Organic Chemistry*; Interscience: New York, 1967; Vol. *4*, pp 93−123.
(52) Dankleff, M. A. P.; Curci, R.; Edwards, J. O.; Pyun, H.-Y. The influence of solvent on the oxidation of thioxane by hydrogen peroxide and by tert-butyl hydroperoxide. *J. Am. Chem. Soc.* **1968**, *90*, 3209−3218.
(53) Edwards, J. O. *Peroxide Reaction Mechanisms*; Interscience Publishers, 1962.
(54) Luo, D.; Smith, S. W.; Anderson, B. D. Kinetics and mechanism of the reaction of cysteine and hydrogen peroxide in aqueous solution. *J. Pharm. Sci.* **2005**, *94*, 304−316.
(55) Alkorta, I.; Elguero, J. Classical versus redox tautomerism: substituent effects on the keto/enol and sulfoxide/sulfenic acid equilibria. *Tetrahedron Lett.* **2004**, *45*, 4127−4129.
(56) Chu, J.-W.; Trout, B. L. On the Mechanisms of Oxidation of Organic Sulfides by H2O2 in Aqueous Solutions. *J. Am. Chem. Soc.* **2004**, *126*, 900−908.
(57) Wiberg, K. B. The Concept of Strain in Organic Chemistry. *Angew. Chem., Int. Ed.* **1986**, *25*, 312−322.
(58) Bayse, C. A. Transition states for cysteine redox processes modeled by DFT and solvent-assisted proton exchange. *Org. Biomol. Chem.* **2011**, *9*, 4748−4751.
(59) Cardey, B.; Enescu, M. A computational study of thiolate and selenolate oxidation by hydrogen peroxide. *ChemPhysChem* **2005**, *6*, 1175−1180.
(60) Winterbourn, C. C.; Metodiewa, D. Reactivity of biologically important thiol compounds with superoxide and hydrogen peroxide. *Free Radicals Biol. Med.* **1999**, *27*, 322−328.
(61) Hamlin, T. A.; Swart, M.; Bickelhaupt, F. M. Nucleophilic substitution (Sn2): Dependence on nucleophile, leaving group, central atom, substituents, and solvent. *ChemPhysChem* **2018**, *19*, 1315.
(62) Claiborne, A. L.; Miller, H.; Parsonage, D.; Ross, R. P. Protein-sulfenic acid stabilization and function in enzyme catalysis and gene regulation. *FASEB J.* **1993**, *7*, 1483−1490.
(63) Winterbourn, C. C. The Biological Chemistry of Hydrogen Peroxide. In *Methods in Enzymology*; Elsevier, 2013; Vol. *528*, pp 3−25.
(64) Barton, J. P.; Packer, J. E.; Sims, R. J. Kinetics of the reaction of hydrogen peroxide with cysteine and cysteamine. *J. Chem. Soc., Perkin Trans. 2* **1973**, 1547−1549.
(65) Radi, R.; Beckman, J. S.; Bush, K. M.; Freeman, B. A. Peroxynitrite oxidation of sulfhydryls. The cytotoxic potential of superoxide and nitric oxide. *J. Biol. Chem.* **1991**, *266*, 4244−4250.

https://dx.doi.org/10.1021/acs.jpcb.0c07510
J. Phys. Chem. B XXXX, XXX, XXX−XXX